Anal. Chem. **1999,** *71,* 2657−2666

Retention and Efficiency in Frit-Inlet Asymmetrical Flow Field-Flow Fractionation

Myeong Hee Moon,*,† P. Stephen Williams,‡ and Hansun Kwon†

Department of Chemistry, Kangnung National University, Kangnung, Korea 210-702, and Department of Chemistry and Geochemistry, Colorado School of Mines, Golden, Colorado 80401

Sample relaxation in the frit-inlet asymmetrical flow field-flow fractionation (FIA-FlFFF) channel is accomplished hydrodynamically. The focusing/relaxation procedure, which is essential to the efficient operation of conventional asymmetrical flow FFF, is therefore avoided. It follows that for FIA-FlFFF there is no requirement for valve switching to achieve convergent (focusing) channel flows, and sample relaxation and separation proceed without interruption. This represents a major advance in the facility of operation of asymmetrical flow FFF. In this work, we present the derivation of equations to describe the variation in mean channel flow velocity along the full length of the frit-inlet asymmetrical channel. Equations for channel void time (the time for a nonretained material to pass through the channel) are also presented. The equations are sufficiently general so as to be applicable to both rectangular and trapezoidal channel designs. On the basis of these equations, the retention time for a sample component can be calculated by applying basic flow FFF theory. Simple equations are also presented to determine conditions consistent with complete relaxation of samples within the frit-inlet region. Such conditions ensure maximization of separation efficiency during subsequent elution. The retention and resolving power of FIA-FlFFF are demonstrated using sets of standard latex spheres and proteins. Experimental data show that retention in FIA-FlFFF follows the general principles of field-flow fractionation, provided the variation in flow velocity is correctly accounted for. Finally, effects of sample load and injection volume are also discussed.

In flow field-flow fractionation (FlFFF), particles or macromolecules are separated within a flow of fluid that is driven along a thin channel of rectangular cross section. The separation is achieved by exploiting differences in diffusion coefficients.[1−5] During its migration along the channel, the sample is carried across the thin dimension of the channel toward the so-called accumulation wall by a secondary cross-flow of the suspending fluid. (It is this secondary flow of fluid that is the defining characteristic of FlFFF. Other forms of field-flow fractionation utilize various applied fields to drive the sample materials toward the accumulation wall.) In FlFFF, this accumulation wall is necessarily permeable and must be overlaid with a semipermeable membrane to prevent the passage of sample materials through the wall. In the case of symmetrical flow FFF, the opposite wall (the depletion wall) is also permeable and the exiting flow at the accumulation wall is exactly matched by an inflow at this depletion wall. In asymmetrical flow FFF, the depletion wall is impermeable and during the separation process all fluid entering the channel does so via the channel inlet. In either case, sample components of different sizes exhibit different diffusional transports away from the resulting region of increased concentration adjacent to the accumulation wall. The counterbalancing of the drag of the cross-flow and the opposing diffusional transport result in a steady state concentration distribution that is unique to each particle size. Their entrainment in the nonuniform (parabolic) longitudinal flow component within the thin FlFFF channel results in their migrations at different mean velocities along the channel length. Those components that have relatively small diffusion coefficients form thin distributions close to the accumulation wall and are carried by relatively slow-moving streamlines, while those with higher diffusion coefficients form thicker distributions, sample a wider range of stream velocities, and are therefore carried more quickly along the channel.

For the attainment of optimum differential transport of sample materials, a relaxation toward steady state transverse distribution of the sample components must be established before their longitudinal migration is initiated. In a conventional symmetrical flow channel, this is normally achieved by stopping the longitudinal channel flow for a short period of time, allowing the cross-flow to bring about relaxation, and then restarting the longitudinal flow to bring about the separation.[6] In an asymmetrical flow FFF system, relaxation is allowed to occur at the stagnation point between the two convergent focusing flow streams originating at the channel inlet and outlet.[7,8] (During sample introduction and

† Kangnung National University.
‡ Colorado School of Mines.

(1) Giddings, J. C. *Science* **1993**, *260*, 1456−1465.
(2) Martin, M.; Williams, P. S. In *Theoretical Advancement in Chromatography and Related Separation Techniques*; Dondi, F., Guiochon, G., Eds.; NATO ASI Series C, Mathematical and Physical Sciences, Vol. 383; Kluwer Academic Publishers: Dordrecht, The Netherlands, 1992; pp 513−580.
(3) Myers, M. N. *J. Microcolumn Sep.* **1997**, *9*, 151−162.
(4) Ratanathanawongs, S. K.; Giddings, J. C. In *Chromatography of Polymers: Characterization by SEC and FFF*; Provder, T., Ed.; ACS Symposium Series 521, American Chemical Society: Washington, DC, 1993; pp 13−29.
(5) Lee, S.; Rao, S. P.; Moon, M. H.; Giddings, J. C. *Anal. Chem.* **1996**, *68*, 1545−1549.
(6) Hovingh, M. E.; Thompson, G. E.; Giddings, J. C. *Anal. Chem.* **1970**, *42*, 195−203.
(7) Wahlund, K.-G.; Giddings, J. C. *Anal. Chem.* **1987**, *59*, 1332−1339.
(8) Wahlund, K.-G.; Litzén, A. *J. Chromatogr.* **1989**, *461*, 73−87.

10.1021/ac990040p CCC: $18.00
Published on Web 06/04/1999

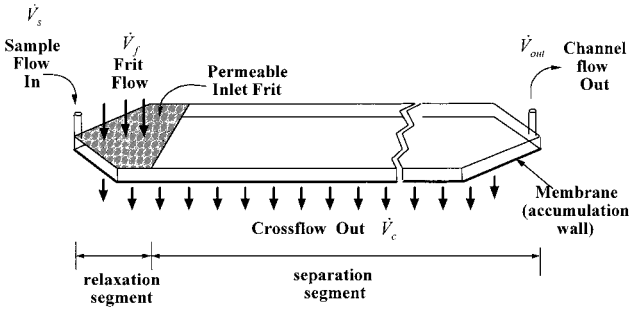

Figure 1. Structure of FIA-FlFFF channel.

relaxation, flow is therefore reversed at what is normally the channel outlet.) In both cases, the longitudinal migration of the sample is interrupted, and during this interruption, the sample is carried toward the accumulation wall. During these static relaxation procedures, the sample materials are therefore susceptible to adsorption on the membrane. Depending on the nature of the sample, the membrane, and the carrier fluid, this can sometimes be a significant problem. Hydrodynamic relaxation[9−12] was proposed as an alternative to the stop-flow procedure used in symmetrical FFF. This technique has the advantage of keeping the sample in motion during relaxation, thereby reducing the tendency for its adsorption while at the same time avoiding the inconvenience of implementing the stop-flow procedure. Two different instrument designs have been used for hydrodynamic relaxation: the split-inlet and the frit-inlet designs. In both cases, the sample is introduced into the lesser of two inlet flows, with the larger contribution to channel flow being introduced to the channel adjacent to the depletion wall. The merging of the two contributions results in the sample being driven into a thin lamina adjacent to the accumulation wall. The sample components are therefore carried by the flow of fluid into a distribution that is close to their final steady-state distributions.

The frit-inlet asymmetrical flow FFF (FIA-FlFFF) system has recently been under development.[13,14] Because it makes use of hydrodynamic relaxation, its operation does not require a separate relaxation procedure even though the channel system is of the asymmetrical type. Hydrodynamic sample relaxation is achieved in the FIA-FlFFF channel by the action of a supplementary flow through a small permeable frit element mounted in the depletion wall near the injection port, as shown in Figure 1. In this modified channel, sample components introduced at the channel inlet are initially distributed across the full thickness of the channel. However, they quickly encounter the relatively fast flowing streams passing through the inlet frit and are driven toward the accumulation wall. While they are being hydrodynamically relaxed by this frit flow, they are continuously carried to the separation segment for separation. Thus the system operation requires only a simple one-step injection procedure, with no need for valve switching or interruption of flow. Its operation is therefore far simpler and more convenient than that of the conventional design.

The initial evaluation of the FIA-FlFFF channel has shown that the system is capable of separating PS standard latex particles to high resolution in both the normal and steric operating modes of FFF.[13] A recent work has also shown the successful separation of several proteins.[14] While these works demonstrated the feasibility of the frit-inlet asymmetrical channel and established the effectiveness of hydrodynamic relaxation, they did not include a theoretical consideration of the rather complicated movement of flow streams in the channel. To realize the full potential of FIA-FlFFF as a separation and characterization technique, the mechanism of sample retention must be clearly understood, and this necessitates a determination of the variation of flow velocities along the full length of the channel. We expect the following qualitative behavior. The mean flow velocity along the channel length will initially fall as the breadth of the inlet endpiece increases. For typical operating conditions, this initial fall will be subsequently reversed due to the contribution of fluid entering the channel via the frit element. In the case of a rectangular channel of constant breadth, the mean flow velocity will decrease downstream of the frit element as fluid is lost via the accumulation wall. This latter reduction in mean fluid velocity may be partially offset or even reversed, depending on flow rate conditions, by tapering the channel breadth. This is most simply implemented using a linear reduction in breadth as in the trapezoidal channel.[15,16] An exponential reduction in breadth has also been proposed[17] for which flow conditions may be set up to maintain constant velocity along this part of the channel. Finally, there will be an increase in mean fluid velocity with the narrowing of the outlet endpiece.

The variation in the velocity of migration must be established throughout the system in order to predict the retention time of a sample component in FIA-FlFFF. Conversely, this information is also required to extract diffusion coefficient and particle size information from observed retention times. In this report, equations for the channel flow velocity in FIA-FlFFF are derived for each segment of the channel. These equations allow calculation of the void time, which is fundamental to both the prediction of retention time and the extraction of information from observed retention times. Experimentally observed data are compared with flow FFF retention theory on on the basis of these derived equations. Overloading effects in the FIA-FlFFF system are also studied by varying the sample mass and injection volume.

THEORY

Void Time Calculation. When an asymmetrical flow FFF system is operated using a frit inlet for hydrodynamic relaxation, injected sample materials undergo the relaxation process without interruption of their migration down the channel. We shall refer to the region of the channel beneath the frit element in the depletion wall as the relaxation segment and the region from the frit to the channel outlet as the separation segment. As they pass beyond the relaxation segment, the separation process begins. The retention for the separation segment (see Figure 1) is expected to be equivalent to that observed in a conventional

(9) Giddings, J. C. *Anal. Chem.* **1985**, *57*, 945−947.
(10) Lee, S.; Myers, M. N.; Giddings, J. C. *Anal. Chem.* **1989**, *61*, 2439−2444.
(11) Giddings, J. C. *Anal. Chem.* **1990**, *62*, 2306−2312.
(12) Liu, M.-K.; Williams, P. S.; Myers, M. N.; Giddings, J. C. *Anal. Chem.* **1991**, *63*, 2115−2122.
(13) Moon, M. H.; Kwon, H. S.; Park, I. *Anal. Chem.* **1997**, *69*, 1436−1440.
(14) Moon, M. H.; Kwon, H. S.; Park, I. *J. Liq. Chromatogr.* **1997**, *20*, 2803−2814.
(15) Litzén, A.; Wahlund, K.-G. *Anal. Chem.* **1991**, *63*, 1001−1007.
(16) Litzén, A. *Anal. Chem.* **1993**, *65*, 461−470.
(17) Williams, P. S. *J. Microcolumn Sep.* **1997**, *9*, 459−467.

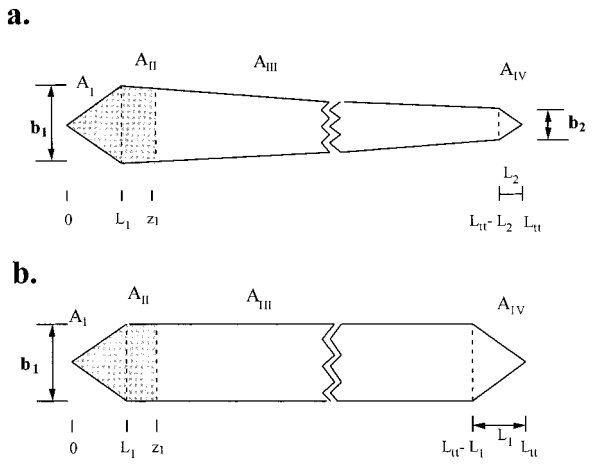

Figure 2. Illustration of channel geometries: (a) trapezoidal; (b) rectangular. Area of each subsegment is represented with A_I–A_{IV}.

asymmetrical channel system, provided complete hydrodynamic relaxation can be achieved. Retention in the separation segment of the FIA-FlFFF channel will follow basic FFF principles as described by the retention ratio, R, given by[18,19]

$$R = t^0/t_r = 6\lambda(\coth(1/2\lambda) - 2\lambda) \tag{1}$$

where t^0 is the void time and t_r is the retention time for this section of the channel, λ is the dimensionless FFF retention parameter that describes the ratio of the mean zone layer thickness l of a sample component to the channel thickness w. The mean layer thickness l is the distance of the center of gravity of the sample zone from the channel wall and is the measure of balance between the applied field force (field strength) exerted on the sample materials and their Brownian motion. Thus, experimental observation of retention time in flow FFF under known field strength and flow rate conditions can provide information on hydrodynamic radius of sample molecules or particles. In all cases, void time must be accurately determined for the channel geometry and flow rates utilized.

The calculation of void time in a conventional symmetrical FFF channel is relatively straightforward since the mean flow velocities in the channel are constant and well-known in most cases. However, in FIA-FlFFF, the calculation is not so simple. There is a merging of two inlet flows (the sample flow entering from effectively a point source at the channel inlet and the frit flow entering uniformly over a small region of the channel depletion wall close to the inlet) with the simultaneous loss of fluid from the system by flow through the membrane on the accumulation wall. As a result, channel flow velocity varies along the axial direction z due to the influx of frit flow and the simultaneous loss of flow through the bottom frit of the channel. The determination of void time therefore requires a careful consideration of the variation in mean flow velocity along the channel. In FIA-FlFFF, two types of channel geometries have been utilized: rectangular and trapezoidal, as shown in Figure 2. The determination of void time can be approached through a consideration of trapezoidal channel dimensions, and the derived formula can be simply adapted for the rectangular channel. In Figure 2a, the dimension of a trapezoidal channel is described by a tip-to-tip channel length L_{tt}, initial breadth b_1, final breadth b_2, lengths of triangular endpieces L_1 and L_2, and length of inlet frit z_1 (with $z_1 > L_1$, although this need not necessarily be so). In the case of a rectangular channel (Figure 2b), channel breadth is constant so that b_2 is equal to b_1 and usually L_2 is also equal to L_1.

The transverse flow velocity close to the accumulation wall u_0 (where the sample materials accumulate and migrate along the length of the channel) can be calculated if it is assumed that the outgoing crossflow is uniform throughout the channel. This velocity is directed toward the accumulation wall and is therefore negative. Its absolute value is given by

$$|u_0| = \frac{\dot{V}_c}{A_c} \tag{2}$$

where $\dot{V}_c$ is the volumetric flow rate of the outgoing crossflow and A_c is the total area of the channel accumulation wall. For a trapezoidal channel A_c is given by

$$A_c = [b_1(L_{tt} - L_2) + b_2(L_{tt} - L_1)]/2 \tag{3}$$

Equation 3 holds for both types of channels but reduces to bL in the case of a rectangular channel, where b is the uniform breadth ($b = b_1 = b_2$) and L is an effective channel length ($L = L_{tt} - L_1$ when $L_1 = L_2$). The void volume, V^0, for both the trapezoidal and rectangular channel is given by

$$V^0 = A_c w \tag{4}$$

The variable channel breadth, $b(z)$, within each segment (I–IV as shown in Figure 2) of a trapezoidal channel is expressed variously as

$$b_I(z) = \frac{b_1}{L_1} z \qquad (0 \le z \le L_1) \tag{5}$$

$$b_{II}(z) = b_{III}(z) = b_1 - \frac{b_1 - b_2}{L_{tt} - L_1 - L_2}(z - L_1) \qquad (L_1 \le z \le L_{tt} - L_2) \tag{6}$$

$$b_{IV}(z) = \frac{b_2}{L_2}(L_{tt} - z) \qquad (L_{tt} - L_2 \le z \le L_{tt}) \tag{7}$$

The subscripts I–IV refer to the four successive channel segments, as shown in Figure 2. The area of accumulation wall up to an arbitrary point z is calculated for each of the four segments by

(18) Giddings, J. C.; Yang, F. J. F.; Myers, M. N. *Anal. Chem.* **1976**, *48*, 1126–1132.
(19) Moon, M. H.; Giddings, J. C. *J. Pharm. Biomed. Sci.* **1993**, *11*, 911–20.

integration of eqs 5−7 as required. These areas are given by

$$A_{\mathrm{I}}(z) = \int_0^z b_{\mathrm{I}}(z)\,\mathrm{d}z = \frac{b_1}{2L_1}z^2 \qquad (0 \le z \le L_1) \tag{8}$$

$$A_{\mathrm{II}}(z) = \int_{L_1}^z b_{\mathrm{II}}(z)\,\mathrm{d}z = b_1(z - L_1) - \frac{b_1 - b_2}{L_{\mathrm{tt}} - L_1 - L_2}\frac{(z - L_1)^2}{2} \qquad (L_1 \le z \le z_1) \tag{9}$$

$$A_{\mathrm{III}}(z) = \int_{z_1}^z b_{\mathrm{III}}(z)\,\mathrm{d}z = b_1(z - z_1) - \frac{b_1 - b_2}{L_{\mathrm{tt}} - L_1 - L_2} \times \left[\frac{(z - L_1)^2}{2} - \frac{(z_1 - L_1)^2}{2}\right] \qquad (z_1 \le z \le L_{\mathrm{tt}} - L_2) \tag{10}$$

$$A_{\mathrm{IV}}(z) = \int_{L_{\mathrm{tt}}-L_2}^z b_{\mathrm{IV}}(z)\,\mathrm{d}z = \frac{b_2}{2L_2}[{L_2}^2 - (L_{\mathrm{tt}} - z)^2] \qquad (L_{\mathrm{tt}} - L_2 \le z \le L_{\mathrm{tt}}) \tag{11}$$

The area of inlet frit, A_{f}, is the sum of the total areas of A_{I} and A_{II} and is given by

$$A_{\mathrm{f}} = A_{\mathrm{I}}(L_1) + A_{\mathrm{II}}(z_1) = \frac{b_1 L_1}{2} + b_1(z_1 - L_1) - \frac{b_1 - b_2}{L_{\mathrm{tt}} - L_1 - L_2}\frac{(z_1 - L_1)^2}{2} \tag{12}$$

In the case of a rectangular channel, this reduces to $b(z_1 - L_1/2)$. The total area of channel accumulation wall is the sum of the total areas of all four segments:

$$A_{\mathrm{c}} = A_{\mathrm{I}}(L_1) + A_{\mathrm{II}}(z_1) + A_{\mathrm{III}}(L_{\mathrm{tt}} - L_2) + A_{\mathrm{IV}}(L_{\mathrm{tt}}) \tag{13}$$

and the result reduces to eq 3, as expected.

The void time, t^0, for any FFF channel is calculated from[8]

$$t^0 = \int_0^L \frac{\mathrm{d}z}{\langle v\rangle(z)} \tag{14}$$

where $\langle v\rangle(z)$ is the local mean flow velocity along the z axis. For the FIA-FlFFF channel, we therefore require the variation of $\langle v\rangle(z)$ along each segment of the channel. Volumetric channel flow rate at any arbitrary point z in segment I is the sum of the sample flow rate I and the fraction of frit flow rate $\dot{V}_{\mathrm{s}}$ up to this point, minus the fraction of crossflow rate $\dot{V}_{\mathrm{f}}$ exiting the channel up to this point. The result may be expressed as

$$\dot{V}_{\mathrm{I}}(z) = \dot{V}_{\mathrm{s}} + \dot{V}_{\mathrm{f}}A_{\mathrm{I}}(z)/A_{\mathrm{f}} - \dot{V}_{\mathrm{c}}A_{\mathrm{I}}(z)/A_{\mathrm{c}} = \dot{V}_{\mathrm{s}} + \Delta|u|A_{\mathrm{I}}(z) \qquad (0 \le z \le L_1) \tag{15}$$

where $\Delta|u| = ((\dot{V}_{\mathrm{f}}/A_{\mathrm{f}}) - (\dot{V}_{\mathrm{c}}/A_{\mathrm{c}}))$ and is the difference between the transverse fluid velocity at the frit $|u_1|$ and at the accumulation wall $|u_0|$.

The local flow rates within the other segments are similarly obtained and are given by

$$\dot{V}_{\mathrm{II}}(z) = \dot{V}_{\mathrm{I}}(L_1) + \dot{V}_{\mathrm{f}}A_{\mathrm{II}}(z)/A_{\mathrm{f}} - \dot{V}_{\mathrm{c}}A_{\mathrm{II}}(z)/A_{\mathrm{c}} = \dot{V}_{\mathrm{s}} + \Delta|u|(A_{\mathrm{I}}(L_1) + A_{\mathrm{II}}(z)) \qquad (L_1 \le z \le z_1) \tag{16}$$

$$\dot{V}_{\mathrm{III}}(z) = \dot{V}_{\mathrm{s}} + \Delta|u|A_{\mathrm{f}} - \dot{V}_{\mathrm{c}}A_{\mathrm{III}}(z)/A_{\mathrm{c}} = \dot{V}_{\mathrm{s}} + \dot{V}_{\mathrm{f}} - \dot{V}_{\mathrm{c}}(A_{\mathrm{f}} + A_{\mathrm{III}}(z))/A_{\mathrm{c}} \qquad (z_1 \le z \le L_{\mathrm{tt}} - L_2) \tag{17}$$

$$\dot{V}_{\mathrm{IV}}(z) = \dot{V}_{\mathrm{s}} + \dot{V}_{\mathrm{f}} - \dot{V}_{\mathrm{c}}(A_{\mathrm{f}} + A_{\mathrm{III}}(L_{\mathrm{tt}} - L_2) + A_{\mathrm{IV}}(z))/A_{\mathrm{c}} \qquad (L_{\mathrm{tt}} - L_2 \le z \le L_{\mathrm{tt}}) \tag{18}$$

In the case of $z = L_{\mathrm{tt}}$, eq 18 yields $\dot{V}_{\mathrm{s}} + \dot{V}_{\mathrm{f}} - \dot{V}_{\mathrm{c}}$ which is equivalent to $\dot{V}_{\mathrm{out}}$, the actual flow rate that can be measured at the outlet of the channel. The local mean flow velocity within each segment of the FIA-FlFFF channel is simply the local volumetric flow rate divided by the local cross sectional area:

$$\langle v\rangle(z) = \frac{\dot{V}(z)}{wb(z)} \tag{19}$$

Substituting eq 19 into eq 14 and making use of eqs 5 and 15 within the interval from $z = 0$ to L_1, we may calculate the passage time for a nonretained material along segment I as

$$t_{\mathrm{I}}^0 = \int_0^{L_1}\frac{\mathrm{d}z}{\langle v\rangle_{\mathrm{I}}(z)} = \int_0^{L_1}\frac{wb_{\mathrm{I}}(z)\,\mathrm{d}z}{\dot{V}_{\mathrm{I}}(z)} = \frac{w}{\Delta|u|}\int_{z=0}^{z=L_1}\frac{\mathrm{d}\dot{V}_{\mathrm{I}}(z)}{\dot{V}_{\mathrm{I}}(z)} = \frac{w}{\Delta|u|}\ln\left(\frac{\dot{V}_{\mathrm{I}}(L_1)}{\dot{V}_{\mathrm{s}}}\right) \tag{20}$$

where $\mathrm{d}\dot{V}_{\mathrm{I}}(z) = \Delta|u|\,\mathrm{d}A_{\mathrm{I}}(z) = \Delta|u|b_{\mathrm{I}}(z)\,\mathrm{d}z$ and $\dot{V}_{\mathrm{I}}(L_1)$ represents the volumetric flow rate at $z = L_1$. Likewise, the passage time for a nonretained material along segment II is calculated by integrating eq 14 using eqs 6 and 16 as

$$t_{\mathrm{II}}^0 = \int_{L_1}^{z_1}\frac{\mathrm{d}z}{\langle v\rangle_{\mathrm{II}}(z)} = \frac{w}{\Delta|u|}\int_{z=L_1}^{z=z_1}\frac{\mathrm{d}\dot{V}_{\mathrm{II}}(z)}{\dot{V}_{\mathrm{II}}(z)} = \frac{w}{\Delta|u|}\ln\left(\frac{\dot{V}_{\mathrm{II}}(z_1)}{\dot{V}_{\mathrm{II}}(L_1)}\right) = \frac{w}{\Delta|u|}\ln\left(\frac{\dot{V}_{\mathrm{s}} + \dot{V}_{\mathrm{f}} - \dot{V}_{\mathrm{c}}A_{\mathrm{f}}/A_{\mathrm{c}}}{\dot{V}_{\mathrm{II}}(L_1)}\right) \tag{21}$$

The passage time for a nonretained material along the relaxation segment, t_{rs}^0 (where subscript rs refers to relaxation segment), is therefore given by the sum of eqs 20 and 21. Taking into account that $\dot{V}_{\mathrm{I}}(L_1)$ is equal to $\dot{V}_{\mathrm{II}}(L_1)$ and substituting for w using eq 4, we obtain the result

$$t_{\mathrm{rs}}^0 = \frac{w}{\Delta|u|}\ln\left(\frac{\dot{V}_{\mathrm{II}}(z_1)}{\dot{V}_{\mathrm{s}}}\right) = \frac{V^0 A_{\mathrm{f}}/A_{\mathrm{c}}}{\dot{V}_{\mathrm{f}} - \dot{V}_{\mathrm{c}}A_{\mathrm{f}}/A_{\mathrm{c}}}\ln\left(\frac{\dot{V}_{\mathrm{s}} + \dot{V}_{\mathrm{f}} - \dot{V}_{\mathrm{c}}A_{\mathrm{f}}/A_{\mathrm{c}}}{\dot{V}_{\mathrm{s}}}\right) \tag{22}$$

The calculation of void time in the separation segment, t_{ss}^0, can be similarly calculated from eqs 17 and 18 with eqs 6 and 7,

respectively, as

$$t_{ss}^0 = \frac{V^0}{\dot{V}_c}\ln\left(\frac{\dot{V}_{III}(z_1)}{\dot{V}_{III}(L_{tt}-L_2)}\right) + \frac{V^0}{\dot{V}_c}\ln\left(\frac{\dot{V}_{IV}(L_{tt}-L_2)}{\dot{V}_{IV}(L_{tt})}\right) = \frac{V^0}{\dot{V}_c}\ln\left(\frac{\dot{V}_s + \dot{V}_f - \dot{V}_c A_f/A_c}{\dot{V}_{out}}\right) \quad (23)$$

Thus, the total void time throughout the channel is obtained by the sum of eqs 22 and 23 as

$$t^0 = \frac{V^0 A_f/A_c}{\dot{V}_f - \dot{V}_c A_f/A_c}\ln\left(\frac{\dot{V}_s + \dot{V}_f - \dot{V}_c A_f/A_c}{\dot{V}_s}\right) + \frac{V^0}{\dot{V}_c}\ln\left(\frac{\dot{V}_s + \dot{V}_f - \dot{V}_c A_f/A_c}{\dot{V}_{out}}\right) \quad (24)$$

Equation 24 yields t^0 in terms of volumetric flow rates and channel dimensions only. The equation is valid for both trapezoidal and rectangular channels. In fact, it is valid for any geometry, including the exponential channel geometry, provided A_c and A_f are properly determined. In the case of a trapezoidal channel, eqs 3 and 12 are used directly to calculate A_c and A_f. For a rectangular channel, where $b_1 = b_2 = b$ and $L_1 = L_2$, A_c is simply given by bL and A_f by $b(z_1 - L_1/2)$, as mentioned earlier.

Variation of Mean Flow Velocity. In the FIA-FlFFF channel, we have shown that channel flow rate varies with z as described by eqs 15−18. Channel breadth also varies with z, as described by eqs 5−7. Mean channel flow velocity varies with the ratio of volumetric flow rate to channel breadth as shown by eq 19. The qualitative expectations for variation of mean flow velocity along the channel have already been discussed. The quantitative description of mean flow velocity within each segment of the channel may be expressed as follows:

$$\langle v\rangle_I(z) = \frac{\dot{V}_s + \Delta|u|A_I(z)}{wb_I(z)} \quad (25)$$

$$\langle v\rangle_{II}(z) = \frac{\dot{V}_s + \Delta|u|(A_I(L_1) + A_{II}(z))}{wb_{II}(z)} \quad (26)$$

$$\langle v\rangle_{III}(z) = \frac{\dot{V}_s + \dot{V}_f - \dot{V}_c(A_f + A_{III}(z))/A_c}{wb_{III}(z)} \quad (27)$$

$$\langle v\rangle_{IV}(z) = \frac{\dot{V}_s + \dot{V}_f - \dot{V}_c(A_f + A_{III}(L_{tt} - L_2) + A_{IV}(z))/A_c}{wb_{IV}(z)} \quad (28)$$

The ranges of validity of eqs 25−28 correspond to those for eqs 15−18, respectively. Equations 25−28 are valid for both rectangular and trapezoidal channels, provided appropriate expressions are used for the channel dimensions. Indeed, they are written in sufficiently general form as to be applicable to arbitrary geometry. It is only necessary to substitute appropriate functions for variation of A and b with z.

The results of calculations (according to eqs 25−28) of $\langle v\rangle$ along channel length are plotted in Figure 3 for the two channel geometries of typical dimensions. Typical flow conditions are considered, and these are listed in the figure caption. The results

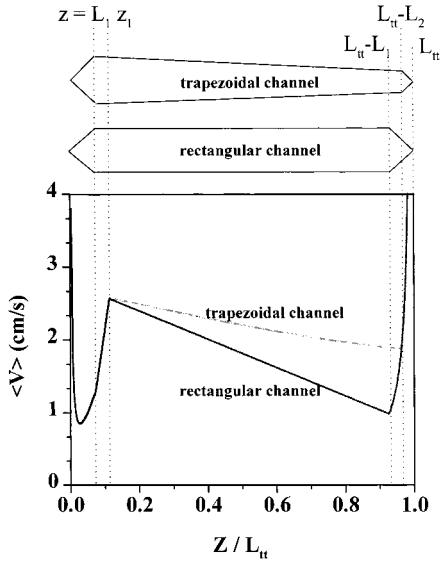

Figure 3. Comparison of linear flow velocities in trapezoidal and rectangular channels. Flow rate conditions are $\dot{V}_s = 0.15$, $\dot{V}_f = 2.4$, $\dot{V}_c = 1.69$, and $\dot{V}_{out} = 0.86$ mL/min. Channel dimensions used for calculation: trapezoidal $L_1 = 2.0$, $L_2 = 1.0$, $b_1 = 2.0$, $b_2 = 1.0$, $z_1 = 3.1$, $L_{tt} = 27.2$ cm, and $w = 78.3$ μm; rectangular $L_1 = L_2 = 2.0$ cm and $b_1 = b_2 = 2.0$ cm with all other dimensions as for trapezoidal channel.

show how the linear flow velocity undergoes substantial variations throughout the channel. The upper curve represents the variation in velocity for the trapezoidal channel and the lower curve that for the rectangular channel. The flow velocity decreases steeply from the inlet for a few millimeters but then increases up to the end of frit-inlet segment at $z = z_1$. Following the relaxation segment, velocity along the rectangular channel decreases as far as the beginning of the triangular endpiece. The variation in velocity along the trapezoidal channel is seen to be far less severe for the same flow rate conditions, as shown by the upper curve. In both cases, the flow velocity finally increases through the outlet endpiece.

Relaxation in FIA-FlFFF. It was mentioned earlier that, to maximize the efficiency of separation along the separation segment of the channel, it is necessary that the sample be fully relaxed within the relaxation segment. A previous work[12] on hydrodynamic relaxation took an approach to optimization of the flow rate ratio $\dot{V}_s/\dot{V}_f$ based on minimizing the sum of the contributions to plate height due to sample volume and to residual relaxation (following incomplete hydrodynamic relaxation). The approach did not take into account the contribution to band spreading that occurs during hydrodynamic relaxation within the relaxation segment. This contribution is rather difficult to calculate, although a recent work[20] has made some progress in this area through a three-dimensional modeling of the fluid flow within the frit inlet. Neither of these works considered the influence of field strength (in our case, the crossflow) in the relaxation segment. When this is taken into account, it becomes apparent that the problem of residual relaxation may be eliminated. In the case of flow FFF, where the relaxation trajectories are independent of particle size and density, the approach is particularly simple. Conditions may be set up to obtain complete relaxation of all particles within the relaxation

(20) Vauthier, J.-C.; Williams, P. S. *J. Chromatogr. A* **1998**, *805*, 149−160.

Table 1. Dimensions of Channel Systems Utilized in This Work[a]

channel system	type	b_1 (cm)	b_2 (cm)	L_1 (cm)	L_2 (cm)	spacer thickness (μm)	A_f (cm^2)	A_c (cm^2)
I	rectangular	2.0		2.0		115	4.20	50.4
II	trapezoidal	2.0	1.0	2.0	1.0	254	4.18	38.8
III	rectangular	1.5		1.5		254	3.53	38.6

[a] All channels have identical tip-to-tip lengths (L_{tt} = 27.2 cm).

segment. The remaining problem of optimizing conditions to minimize the sum of plate height contributions due to sample volume and to the relaxation process is a far more complicated task that is certainly beyond the scope of this work.

Just prior to the frit element, the sample will be distributed across the full thickness of the channel. To a good approximation, complete relaxation will be achieved within the relaxation segment provided a particle that enters the channel adjacent to the frit element (the furthest possible distance from the accumulation wall) follows a trajectory through the relaxation segment that takes it to the accumulation wall at $z = z_1$, directly below the end of the frit element. Other particles that are initially closer to the accumulation wall will take less time to be carried to the wall. Their longitudinal migration during relaxation will therefore be smaller than z_1. For such conditions, we can assume that the sample will be fully relaxed before entering the separation segment. A consideration of this limiting trajectory indicates that these conditions correspond to

$$\dot{V}_s = \dot{V}_c A_f / A_c \tag{29}$$

It follows that, provided $\dot{V}_s \leq \dot{V}_c A_f / A_c$, the sample will be fully relaxed in the relaxation segment. Incidentally, if conditions are set up according to eq 29, the equation for void time reduces to

$$t^0 = \frac{\dot{V}_s}{\dot{V}_f - \dot{V}_s}\frac{V^0}{\dot{V}_c}\ln\left(\frac{\dot{V}_f}{\dot{V}_s}\right) + \frac{V^0}{\dot{V}_c}\ln\left(\frac{\dot{V}_f}{\dot{V}_{out}}\right) \tag{30}$$

The time for the particle to follow the limiting trajectory from the frit to the accumulation wall may be considered to be a very good approximation to the relaxation time τ. We shall assume that this time does indeed correspond to the relaxation time, in which case

$$\tau = w\int_1^0 \frac{dx/w}{u(x/w)} \tag{31}$$

where $u(x/w)$ is given by[21]

$$u(x/w) = u_0 + (u_1 - u_0)(3(x/w)^2 - 2(x/w)^3) \tag{32}$$

in which $u_0 = -\dot{V}_c/A_c$ and $u_1 = -\dot{V}_f/A_f$. Equation 32 requires numerical solution if $u_1 \neq 0$ and $u_1 \neq u_0$. From eqs 31 and 32 we obtain

$$\tau = \frac{w}{|u_0|}\int_0^1 \frac{dx/w}{1 + (|u_1|/|u_0| - 1)(3(x/w)^2 - 2(x/w)^3)} \tag{33}$$

and we see that τ is related to $w/|u_0|$ (which is equal to $V^0/\dot{V}_c$) and $|u_1|/|u_0|$ (equal to $\dot{V}_f A_c/\dot{V}_c A_f$), provided relaxation does indeed take place within the relaxation segment.

It is interesting to consider the likely range of $|u_1|/|u_0|$ and the consequent range of the integral in eq 33. We can say that it would be a very unusual, although not impossible, set of conditions where $\dot{V}_{out} < \dot{V}_s$. So, if we set $\dot{V}_s$ as a lower limit for $\dot{V}_{out}$, it must follow that $\dot{V}_f \geq \dot{V}_c$. From this, it must then follow that $|u_1|/|u_0| \geq A_c/A_f$. For the channel dimensions listed in Table 1, A_c/A_f ranges from 9.3 to 12. The specific ratio in each case must correspond to the lowest ratio of $|u_1|/|u_0|$ that may be used to obtain $\dot{V}_{out} \geq \dot{V}_s$. It is possible that other channels may be constructed in the future for which A_c/A_f is larger. Even so, we might reasonably expect $|u_1|/|u_0|$ to fall in the approximate range 10−50. The integral in eq 33 takes the values of 0.311, 0.218, and 0.136 for $|u_1|/|u_0|$ of 10, 20, and 50, respectively.

We can carry out a comparison of relaxation time τ with relaxation segment void time t^0_{rs} as follows. From a consideration of eq 29, it may be shown that relaxation will be completed within the relaxation segment, provided $\dot{V}_f/\dot{V}_s \geq |u_1|/|u_0|$. It follows that, for the limiting conditions consistent with eq 29, the relaxation segment void time is given by

$$t^0_{rs} = \frac{w}{|u_0|}\frac{1}{(|u_1|/|u_0| - 1)}\ln\left(\frac{|u_1|}{|u_0|}\right) \tag{34}$$

Both τ and limiting t^0_{rs} are therefore dependent on just $w/|u_0|$ and $|u_1|/|u_0|$. We see that $t^0_{rs}|u_0|/w = 0.256$, 0.158, and 0.0798 for $|u_1|/|u_0| = 10$, 20, and 50, respectively. It is apparent that τ tends to be a little larger than limiting t^0_{rs}, although they are similar in magnitude.

Retention Time in FIA-FlFFF. When hydrodynamic relaxation in FIA-FlFFF is successfully achieved, the elution of sample components along the separation segment of the channel should follow FFF principles. Thus, retention time for the separation segment $t_{r,ss}$ in FIA-FlFFF may be predicted from the void time for the separation segment t^0_{ss} and the expression for retention ratio as given by eq 1. Therefore, we have

$$t_{r(ss)} = \frac{t^0_{ss}}{6\lambda(\coth(1/2\lambda) - 2\lambda)} \tag{35}$$

(21) Giddings, J. C. *Sep. Sci. Technol.* **1986**, *21*, 831−843.

in which, for flow FFF, λ is given by

$$\lambda = \frac{D}{w^2}\frac{V^0}{\dot{V}_c} \tag{36}$$

In the above equation, D is the diffusion coefficient of the sample component. For a highly retained component, eq 35 reduces to $t_{r(ss)} \cong t^0_{ss}/6\lambda$. A complication remains. As described earlier, we may set up conditions to ensure sample relaxation prior to the separation segment, as consistent with eq 29. If such conditions are set, then following the short relaxation time the sample will be spread nonuniformly over the accumulation wall below the frit element, from the inlet (assuming negligible FFF migration for the relaxed portion of the sample during the relaxation time) to $z = z_1$. (In fact, the sample will be swept away from the apex of the endpiece by the very fast flow velocity in this region.) A simple center of gravity of the zone at this point in time cannot be taken as the starting point for FFF elution. This is because the mean fluid velocity varies in a complicated manner through the relaxation segment. The details of these considerations are beyond the scope of the present work. It will suffice to say that the effective void time t^0_{eff} for FFF elution must fall somewhere between t^0_{ss} and $t^0_{rs} + t^0_{ss}$. We may write

$$t^0_{eff} = ft^0_{rs} + t^0_{ss} \tag{37}$$

where f is the effective fraction of the relaxation segment void time and f lies somewhere between 0 and 1 when conditions are consistent with eq 29. The fraction f increases as either $\dot{V}_s/\dot{V}_c$ or $\dot{V}_s/\dot{V}_f$ decreases. The full retention time is then given by

$$t_r = \tau + \frac{t^0_{eff}}{R} \tag{38}$$

EXPERIMENTAL SECTION

The frit-inlet asymmetrical flow FFF system, built in-house, is identical to that described in earlier reports.[13,14] Three different channels were used in this work, and their dimensions are listed in Table 1. The membranes used as accumulation walls were regenerated cellulose YM-10 and YM-30 having the MW cut-offs of 10 000 and 30 000, respectively (Amicon Co., Beverly, MA). Samples comprised polystyrene latex bead standards having nominal diameters of 0.040, 0.091, 0.135, 0.220, 0.300, and 0.426 μm (Duke Scientific Co., Palo Alto, CA) and the proteins cytochrome *c* (12.4 K), carbonic anhydrase (29 K), BSA (66 K), alcohol dehydrogenase (150 K), apoferritin (443 K), and thyroglobulin (670 K) from Sigma (St. Louis, MO). Samples were introduced into the channel using a model 7725I Rheodyne injection valve (Rheodyne, Cotati, CA). Sample masses of about 1 μg for each particle standard and about 2−3 μg for each protein standard were used.

The carrier solution was prepared from purified (by reverse osmosis) and deionized water. For particle separation, 0.05% SDS was added to the pure water to maintain particle dispersion and 0.02% NaN_3 as a bactericide. The carrier solution for protein separation was Tris-HCl buffer ($I = 0.10$M) adjusted to pH = 7.8. All solutions were passed through a 0.45 μm membrane filter prior to use.

For the delivery of carrier solutions to the FIA-FlFFF channel, two HPLC pumps were used: a Vintage 2000LC pump (OromTech, Seoul, Korea) and an Eldex cc-100-s HPLC pump from Rainin Instrument Co. Inc. (Woburn, MA). Pump control software was obtained from OromTech. Eluted sample materials were monitored using an M720 variable-wavelength UV detector (Young-In Scientific Co. Ltd., Seoul, Korea). The wavelengths used for detection were 254 nm for particles and 280 nm for proteins. Fractogram signals were saved using Chromastar II data acquisition.

RESULTS AND DISCUSSION

It was found by experiment that, for optimum separation, which requires an effective sample relaxation, a small flow rate ratio of $\dot{V}_s/\dot{V}_f$ is required. In practice, a ratio of ~0.05 was found to be generally effective. This is in agreement with our theoretical development. We expect relaxation to be complete within the relaxation segment, provided $\dot{V}_s/\dot{V}_f \le \dot{V}_c A_f/\dot{V}_f A_c = |u_0|/|u_1|$. With the additional requirement that $\dot{V}_{out} \ge \dot{V}_s$, the flow rate requirements may be written in the form

$$\dot{V}_s/\dot{V}_f \le |u_0|/|u_1| \le A_f/A_c \tag{39}$$

and for the channels used in this work A_f/A_c varies from 0.083 to 0.11. The use of a smaller $\dot{V}_s/\dot{V}_f$ than the critical ratio would reduce the contribution to band spreading due to the relaxation process and increase the contribution due to the finite sample volume. As mentioned previously, the optimization of the $\dot{V}_s/\dot{V}_f$ ratio (minimizing the sum of these two contributions to plate height) is beyond the scope of the present work. It is apparently a good practice however to work at a ratio of $\dot{V}_s/\dot{V}_f$ that is a little lower than the critical value.

Determination of conditions for achievement of effective relaxation constitutes just one part of our study. The other concerns the prediction of retention time of materials in the FIA-FlFFF system. We have the problem associated with the fraction f of relaxation segment void time included in eq 37. The accurate determination of f awaits a more thorough study of the fluid dynamics in the relaxation segment. We may certainly estimate its value, taking into account the degree to which $|u_0|/|u_1|$ exceeds $\dot{V}_s/\dot{V}_f$. However, a more serious problem concerns the determination of channel thickness w and consequent void volume V^0. This is a difficulty that is common to all forms of flow FFF at present. Due to the compressibility of the membrane, the channel thickness may differ from that of the channel spacer material. That part of the membrane which lies between the spacer and the block that holds the accumulation wall frit may be compressed, while that part which forms the accumulation wall itself would remain uncompressed. It is therefore common for the channel thickness to be less than that of the channel spacer.

An indirect experimental determination of channel thickness may be made by measuring the retention times of standard

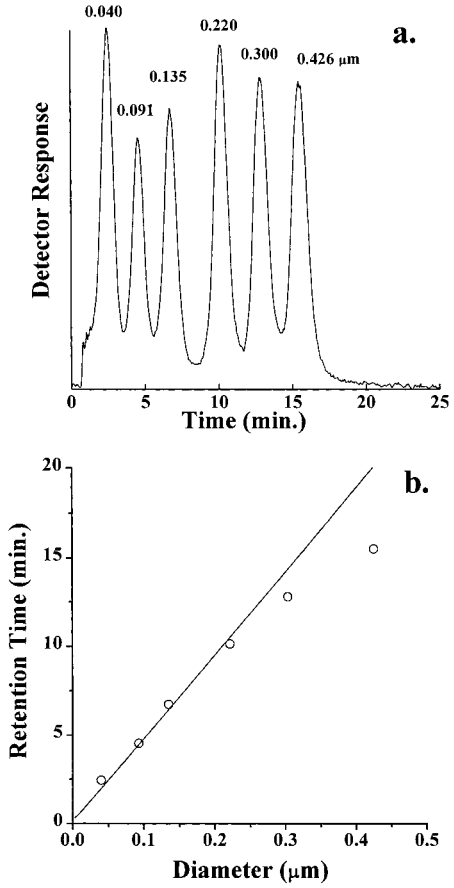

Figure 4. (a) Separation of polystyrene mixtures in FIA-FlFFF by hydrodynamic relaxation obtained at the flow rate conditions used in Figure 3. (b) Correlation of experimental data with the semiempirically obtained theory curve. A rectangular channel (channel I in Table 1) is used.

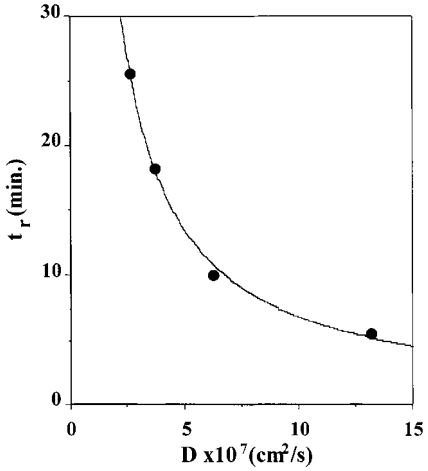

Figure 5. Plot of retention time (t_r) vs diffusion coefficient (D) of four protein standards (carbonic anhydrase, BSA, alcohol dehydrogenase, and apoferritin) with the theory (solid line) calculated semiempirically using eqs 29 with 24 obtained at channel II. Flow rate conditions are $\dot{V}_s = 0.20$, $\dot{V}_f = 7.0$, $\dot{V}_c = 7.0$, and $\dot{V}_{out} = 0.20$ mL/min.

materials. That void volume, and hence channel thickness, which together with the measured flow rate conditions gives a consistency with the observed retention times may be assumed to be correct. To minimize uncertainty, a number of measurements of retention time for different standards under different flow conditions may be made and a best fit for void volume and channel thickness obtained. This indirect approach in fact allows us to ignore the small uncertainties associated with sample migration during relaxation. The fit may be carried out for the separation segment of the channel only, with these uncertainties being accounted for with some small variation of w. This is the approach taken in the work described below. Later, a more sophisticated fitting will undoubtedly be possible.

Figure 4a shows a typical separation of six polystyrene latex standards by FIA-FlFFF obtained using flow conditions of $\dot{V}_s = 0.15$, $\dot{V}_f = 2.4$, $\dot{V}_c = 1.69$, and $\dot{V}_{out} = 0.86$ mL/min with channel system I. For these conditions, $\dot{V}_s/\dot{V}_f = 0.063$ and $\dot{V}_c A_f/\dot{V}_f A_c = 0.059$. Because $\dot{V}_s$ (=0.15 mL/min) was only slightly greater than $V_c A_f/A_c$ (=0.14 mL/min), relaxation is expected to have been very close to complete within the relaxation segment. (Complete relaxation within the relaxation segment is predicted when $\dot{V}_s \leq \dot{V}_c A_f/A_c$, as indicated by eq 29.) This separation of particles having a 10-fold diameter range takes requires 17 min with nearly baseline separation of the mixture components. The separation demonstrates the great capability for high-resolution separations of the FIA-FlFFF channel, run without the static relaxation techniques. When a best fit is obtained for V^0 and w, particle retention in the FIA-FlFFF channel agrees with the retention mechanism of FFF. The relationship between the observed retention time and particle diameter for this run is plotted as the open circles in Figure 4b. The solid line represents the calculated retention time with the assumed channel thickness of 78.3 μm obtained by regression of five data points (PS 0.040−0.300 μm). (Note that this best fit thickness of 78.3 μm is considerably less than the nominal thickness of 115 μm for the spacer material.) The larger particles exhibit some tendency to elute earlier than predicted by ideal theory due to steric and hydrodynamic lift effects. For this reason, the data point for the 0.426 μm particle was excluded from the fitting procedure. It can be seen that, once adjustment is made to V^0 and w, agreement with theoretical prediction is good.

The same procedure was followed for the elution of a mixture of proteins using channel II. A thicker channel spacer was used in constructing channel II. A thicker channel is more suited to the retention of proteins. Their relatively high diffusion coefficients would require very high $\dot{V}_c$ in conjunction with a thin channel (see eq 36). Channel II was also constructed with trapezoidal geometry, the dimensions being listed in Table 1. Figure 5 shows the plot of retention time vs diffusion coefficient for four protein standards obtained under flow conditions of $\dot{V}_s = 0.20$, $\dot{V}_f = 7.0$, $\dot{V}_c = 7.0$, and $\dot{V}_{out} = 0.20$ mL/min. For these conditions, $\dot{V}_s/\dot{V}_f = 0.029$ and $\dot{V}_c A_f/\dot{V}_f A_c = 0.11$. Alternatively, we may compare $\dot{V}_s = 0.20$ mL/min with $\dot{V}_c A_f/A_c = 0.77$ mL/min to see that the protein sample should therefore have been well relaxed within the relaxation segment (see eq 29). In the calculation of the channel thickness, diffusion coefficients for the proteins were used directly for the regression, and the best-fit result of 247 μm was obtained, which is in good agreement with the nominal spacer thickness of 254 μm. Assuming this best-fit channel thickness, the predicted retention time is plotted as the solid line in Figure 5. The agreement with experiment is seen to be very good.

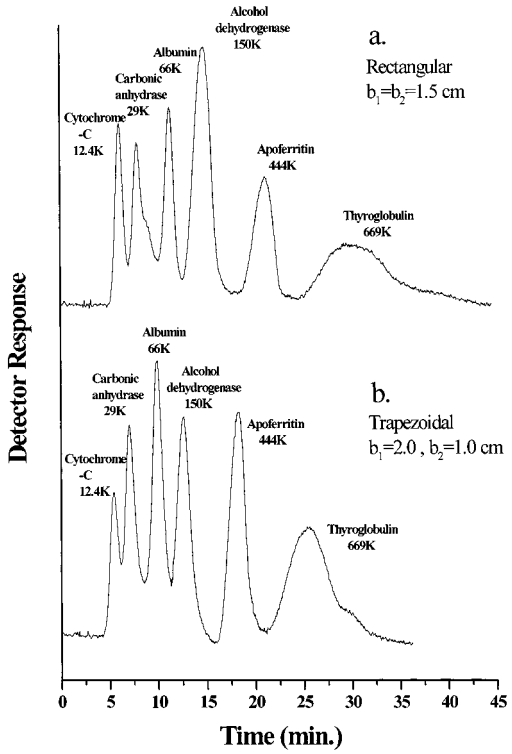

Figure 6. Effect of channel geometry in the separation efficiency in FIA-FlFFF. Flow rate conditions are (a) $\dot{V}_s = 0.20$, $\dot{V}_f = 6.1$, $\dot{V}_c = 6.12$, and $\dot{V}_{out} = 0.14$ mL/min for channel III and (b) $\dot{V}_s = 0.20$, $\dot{V}_f = 7.0$, $\dot{V}_c = 7.0$, and $\dot{V}_{out} = 0.20$ mL/min for channel II.

Retention and efficiency for rectangular and trapezoidal FIA-FlFFF channels are compared in Figure 6. As can be seen from Table 1, the channels have almost identical A_c, and as the same spacer material was used for both, their void volumes are also expected to be almost identical. The run conditions for the two channel systems corresponded to those used to generate the data for Figure 5. Parts a and b of Figure 6 were obtained using channels III and II, respectively. The ratio $\dot{V}_s/\dot{V}_f$ was set to 0.029 for both runs, as for Figure 5. For channel II $\dot{V}_c A_f/\dot{V}_f A_c = 0.11$ (as before), while for channel III $\dot{V}_c A_f/\dot{V}_f A_c = 0.091$. Therefore, sample components were expected to be well relaxed hydrodynamically. In fact, the two fractograms exhibit excellent resolution. The fractogram of Figure 6b however shows somewhat reduced retention times of each component and substantial reduction of peak broadening, particularly for the later eluting peaks. It is possible that the decreasing flow velocity along the rectangular channel allows sample material to contact the accumulation wall more frequently, leading to an increased tendency for adsorption.

Finally, the overloading effect was investigated for the FIA-FlFFF system using carbonic anhydrase. The influence of sample mass on overloading was examined by increasing the mass of anhydrase at a fixed injection volume of 2 μL. The results are shown in Figure 7a. The mass of sample injected for the fractogram shown in Figure 6 corresponded to about 2−3 μg of each protein standard. Figure 7a shows the results for injection masses up to about 10 times this amount (24 μg). There does not seem to be a significant shift in the retention time, but peak broadening results in an increase in σ_t of about 37%. The response scale shown in the figure represents the millivolt readout recorded at a detector sensitivity of 0.01 mV. The peak area does not increase linearly with sample mass, which indicates that there appears to be some problem with recovery. The effect of injection volume on the retention was examined using a fixed sample mass of 3 μg. The results are superimposed in Figure 7b. There appears to be little sensitivity to sample volume for the range studied. Even when the injection volume was increased to 16 μL, the retention time of the carbonic anhydrase sample shifted by only 2%.

CONCLUSIONS

The FIA-FlFFF system is proving remarkably convenient to operate compared to more conventional flow FFF systems (both symmetrical and asymmetrical). There does not appear to be any significant compromise in resolution when flow conditions are set up according to simple guiding equations. Also, when proper account is taken of the variation of mean flow velocity along the channel, retention times should be predictable from first principles.

ACKNOWLEDGMENT

The authors wish to acknowledge financial support from the Korea Research Foundation made in the program year of 1997.

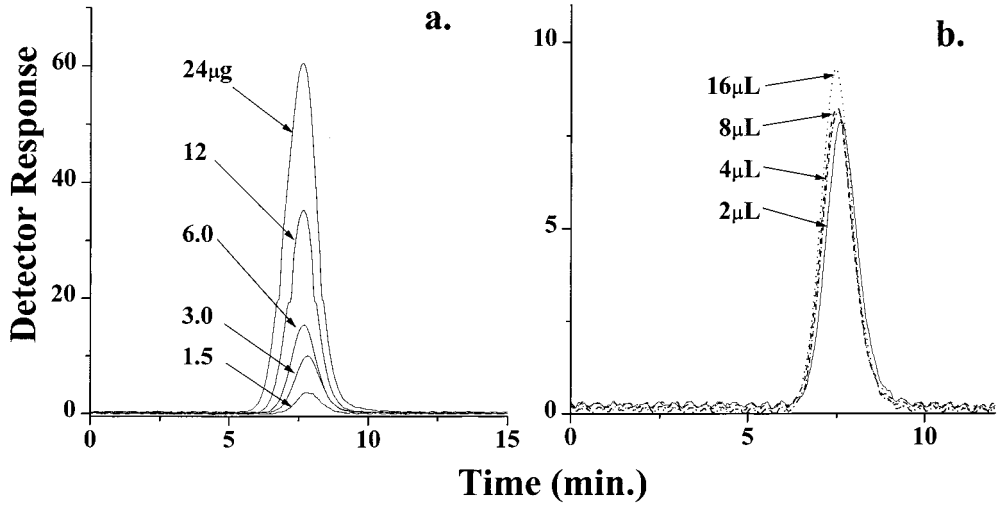

Figure 7. (a) Effect of injection mass on overloading in FIA-FlFFF using carbonic anhydrase. Injection volume is fixed at 2 μL for all runs. (b) Effect of injection volume in using the same sample in as in part a with the fixed sample mass at 3.0 μg. The relative standard deviation in peak area for (b) is 5.6%. Flow rates used: $\dot{V}_s = 0.17$, $\dot{V}_f = 7.0$, $\dot{V}_c = 7.0$, and $\dot{V}_{out} = 0.17$ mL/min. Both runs were obtained using channel II.

GLOSSARY

A_f	area of inlet frit
A_c	total area of channel accumulation wall
$A(z)$	area of channel accumulation wall up to point z
b	channel breadth
b_1	breadth of inlet endpiece
b_2	breadth of outlet endpiece
$b(z)$	local channel breadth
D	diffusion coefficient
f	effective fraction of t_{rs}^0
l	equilibrium thickness of sample zone
L	effective channel length
L_1	length of inlet endpiece
L_2	length of outlet endpiece
L_{tt}	tip-to-tip channel length
t_r	retention time
$t_{r(ss)}$	retention time for separation segment
t^0	channel void time
t_{eff}^0	effective void time
t_{rs}^0	void time for relaxation segment of channel
t_{ss}^0	void time for separation segment of channel
$u(x/w)$	transverse flow velocity as function of x/w
u_0	transverse flow velocity adjacent to accumulation wall
u_1	transverse flow velocity adjacent to frit element
V^0	void volume of channel
$\dot{V}_c$	crossflow rate
$\dot{V}_f$	flow rate of carrier through frit inlet
$\dot{V}_{out}$	flow rate at channel outlet
$\dot{V}_s$	flow rate of sample inlet substream
$\langle v \rangle(z)$	mean local flow velocity
w	channel thickness
z	distance from channel inlet
z_1	length of inlet frit
$\Delta\|u\|$	difference in transverse fluid velocity at frit and at accumulation wall
η	viscosity of carrier solution
λ	dimensionless retention parameter
τ	relaxation time

Received for review January 14, 1999. Accepted April 13, 1999.

AC990040P